Energy Advances

ROYAL SOCIETY OF CHEMISTRY

PAPER

View Article Online
View Journal | View Issue

Cite this: *Energy Adv.*, 2024, 3, 1642

Additive manufacturing of highly conductive carbon nanotube architectures towards carbon-based flexible thermoelectric generators

Christos K. Mytafides, *[ab] William J. Wright,[a] Raden Gustinvil,[a] Lazaros Tzounis,[bc] George Karalis,[b] Alkiviadis S. Paipetis[b] and Emrah Celik*[a]

Moving the fabrication of electronics from the conventional 2D orientation to 3D space, necessitates the use of sophisticated additive manufacturing processes which are capable to deliver multifunctional materials and devices with exceptional spatial resolution. In this study, it is reported the nozzle-guided 3D-printing of highly conductive, epoxy-dispersed, single-walled carbon nanotube (SWCNT) architectures with embedded thermoelectric (TE) properties, capable to exploit significant waste thermal energy from the environment. In order to achieve high-resolution and continuous printing with the SWCNT-based paste through a confined nozzle geometry, *i.e.* without agglomeration and nozzle clogging, a homogeneous epoxy resin-dispersed SWCNT paste was produced. As a result, various 3D-printed structures with high SWCNT concentration (10 wt%) were obtained *via* shear-mixing processes. The 3D printed p- and n-type epoxy-dispersed SWCNT-based thermoelements exhibit high power factors of 102 and 75 μW mK^{-2}, respectively. The manufactured 3D carbon-based thermoelectric generator (3D-CTEG) has the ability to stably operate at temperatures up to 180 °C in ambient conditions (1 atm, relative humidity: 50 ± 5% RH), obtaining TE values of an open-circuit voltage V_{OC} = 13.6 mV, short-circuit current I_{SC} = 1204 μA, internal resistance R_{TEG} = 11.3 Ohm, and a generated power output P_{max} = 4.1 μW at ΔT = 100 K (with T_{Cold} = 70 °C). The approach and methodology described in this study aims to increase the flexibility of integration and additive manufacturing processes for advanced 3D-printed conceptual devices and the development of multifunctional materials.

Received 19th March 2024,
Accepted 26th May 2024

DOI: 10.1039/d4ya00182f

rsc.li/energy-advances

1. Introduction

Among the most urgent concerns we encounter daily are those related to the environment and energy consumption. Vast amounts of energy are lost in terms of heat when it is converted from the primary carriers to the end use. Waste energy generated as heat worldwide by the most prevalent end use sectors including residential, industrial, transportation, and power plants, globally accounts for nearly 72 percent of worldwide energy supply. More specifically, 63 percent of the aforementioned heat energy is generated at temperatures below 100 °C. The power generation field has the highest proportion in this temperature range, followed by industries and transportation.[1]

Better utilization of this excessive thermal energy has the potential to improve the energy efficiency minimizing the consumption. Thermoelectric (TE) generation is a quite promising renewable energy technology with a broad variety of potential applications. Thermal energy conversion to electricity is a sustainable energy source that may be utilized to exploit waste dissipated heat by leveraging the Seebeck effect of thermoelectricity.[2] TE materials with high Seebeck coefficient (S) demonstrate high thermoelectric energy generation since the thermoelectric voltage (V) is related to the temperature variation (ΔT) according to the equation of $S = \Delta V/\Delta T$. In addition, the power factor (PF) is defined as PF = $\sigma \cdot S^2$, where σ is the electrical conductivity and S is the Seebeck coefficient, and is used to measure the efficiency of a TE material.

In addition to high Seebeck coefficient and high electrical conductivity, TE material must have low thermal conductivity to effectively transform waste heat into useful power. A low thermal conductivity is needed to maintain a substantial temperature difference within the material.[3,4] Even though TE materials have the potential to provide an efficient and reliable renewable technology theoretically, the majority of materials

[a] *Advanced Nano Systems Laboratory, Mechanical & Aerospace Engineering Department, University of Miami, 1251 Memorial Drive, FL 33146, Coral Gables, USA. E-mail: cmytafides@gmail.com, e.celik@miami.edu; Tel: +30(695)500-5340, +1(786)819-1831, +1(305)284-9364*
[b] *Composites and Smart Materials Laboratory, Materials Science & Engineering Department, University of Ioannina, GR-45110 Ioannina, Greece*
[c] *Mechanical Engineering Department, Hellenic Mediterranean University, Estavromenos, 71004, Heraklion, Crete, Greece*

that currently render the highest efficiency are costly to produce and are based on components that are rare in nature or/and toxic. Tellurium, bismuth, lead telluride, bismuth telluride, zinc antimonide, silicon, and germanium are some of the most commonly used TE materials.[5,6] Typical thermoelectric materials and module production is a tedious multi-step procedure which comprises material production and synthesis, casting of thermoelements and metal interconnection of these thermoelements which mandates the employment of advanced instrumentation. In addition, this processing method has various limitations, including the fact that it is only adaptable to rectangular designs where a considerable proportion of the active material is lost during the manufacturing process. In addition, large scale integration requires significant amount of time.[7,8] As a result, the cost of thermoelectric energy generation escalates significantly. This is indicative of the fact that there is a lack for commercial demand for thermoelectric generators (TEGs). TEGs have a great potential use in remote energy-harvesting and the supply of power for wireless and portable devices, and they might make a substantial contribution to the field of Internet of Things (IoT). To accomplish these goals, the weight, the design as well as the form-factor of the TE devices (*i.e.* flexibility) become crucially important in addition to the cost and the device performance. This dictates the necessity for simple processes based on low-cost carbon-based TE materials that may be printed in order to manufacture flexible and organic or carbon-based TE devices.[9,10] Currently, TE materials are of great attention from the scientific community and numerous of organic and inorganic materials are being investigated as potential materials for thermoelectric energy-harvesting devices.[11–15]

Additive manufacturing (or 3D printing) technology provide substantial assets in terms of reducing the cost, equipment, time and difficulty of thermoelectric material and device production. Furthermore, it is capable to produce sophisticated and adaptable device geometries as well as flexible and adjustable manufacturing parameters.[6] TE materials may be printed in a layer-by-layer fashion *via* a computer-aided procedure, simplifying the manufacturing process, minimizing the product-waste as well as maximizing the freedom of the shape-printing and device design. Additive manufacturing methods have recently been employed to produce TE materials in the form of thick components or thin films.

Inkjet printing and screen printing, for example, have been shown to be effective methods for effortlessly changing geometrical parameters like size and shape.[6,16–20] However, because of their high porosity, these approaches demonstrate limited power output, high contact resistance between the thermoelements, and poor mechanical characteristics. These limitations can be alleviated by printing thicker and denser components.

TEGs made from bismuth-telluride were created utilizing the screen-printing technology and extrusion-based printing.[21,22] Accordingly, He *et al.* showed the manufacturing of TE bismuth–antimony–telluride nanoparticle-based (NPs) samples in photoresin using stereolithography in ratios containing up to 60% NPs. The 3D-printed thermoelements can mostly consist of NPs after thermal annealing.[23] Stereolithography and dispenser-printing methods are auspicious additive manufacturing processes for the production of thick TE components. Nonetheless, both exhibit inadequate TE efficiency comparing to standard manufacturing processes, with orders of magnitude lower TE characteristics.

Furthermore, selective laser melting (SLM) and sintering (SLS) are two developing technologies that have recently been used to produce thermoelements with complicated shapes and designs.[24,25] These methods rely on the deposition of a thin layer of thermoelectric powder, followed by melting with a laser beam and solidification.[26,27] Notwithstanding the ability to fabricate thermoelectric materials with various shapes, such procedures need a significant initial investment in equipment[28] limiting the adoptability of these manufacturing processes.

Carbon-based printable materials are of great interest as they are inexpensive to produce, they are abundant, non-toxic, and their low density is beneficial for high specific energy output. Single-walled carbon nanotubes (SWCNTs)[29] possess unique electrical, mechanical, and thermal characteristics and they can be prepared inexpensively in the form of conductive or semiconductive inks for the fabrication of printed electronics.[30] SWCNTs are commonly used as additives to increase the conductivity of polymers, which are usually employed for 3D-printing materials. One of the most challenging issues in the field of 3D-printed electronics is determining the optimal printing procedure for manufacturing high resolution 3D structures. Recent studies have demonstrated the fabrication of 3D elements in the scale of micrometer utilizing the ink-based printing techniques. In addition, SWCNTs have attracted particular interest as raw materials for the development of printed electronics and thermoelectric generators.[15,31–33] This is due to both their significant phonon scattering capabilities and their exceptionally high electrical and mechanical properties. Furthermore, SWCNTs have adjustable semiconducting qualities since their n- or p-type behavior may be altered using certain doping techniques, resulting in noteworthy adaptability in terms of TE properties.[34,35]

In this study, it is demonstrated the manufacturing process and the performance of a flexible carbon-based 3D-printed thermoelectric generator (3D-CTEG) approaching a low-cost and versatile production of energy harvesting devices. Single-wall carbon nanotubes (SWCNTs) were used for the production of the printable pastes which were mixed with a flexible epoxy resin to realize self-standing thermoelectric elements, in order to fabricate the 3D-CTEG with significant TE performance. The successful implementation of the carbon-based additively manufactured flexible TE systems, reduces current costs and geometric limitations and allows for a wide range of applications of these materials.

2. Materials and methods

2.1. Preparation of SWCNT-based TE paste

Single-walled carbon nanotubes powder (purity of carbon $\geq$85%) was acquired from OCSiAl (TUBALL™, Russia) with approximately 5 μm length and 1.7 ± 0.5 nm outer mean diameter. The p-type TE ink was produced by a facile epoxy-based

solution/mixing process, by adding SWCNTs and poly(3,4-ethylenedioxythiophene)polystyrene sulfonate (PEDOT:PSS) in the Superflex (flexible-after-curing) epoxy resin (3DMaterials, Korea) as presented in Fig. 1a-c. The mixture of 10 wt% of SWCNTs and 5 wt% of PEDOT:PSS in the epoxy was mixed utilizing the ARM-310 shear mixer (Thinky Corporation, Japan) primarily for 5 minutes, then for another 7 minutes. All mixing processes using the ARM-310 were performed at 2000 rpm, resulting in viscous SWCNT-based thermoelectric inks/pastes of 27 Pa s. The n-type SWCNT-based 3D-printed thermoelement was produced by adding 10 wt% SWCNTs and 10 wt% polyethylenimine (PEI) in the Superflex epoxy resin. In this work, PEI was used as a low-cost, air-stable, and easy to process n-dopant. PEDOT:PSS and PEI were acquired from Sigma-Aldrich (Merck, Germany). After the SWCNT/epoxy-based TE pastes were produced, it were successfully extruded utilizing the direct ink writing (DIW) method as can been seen in Fig. 1a–c, using a 0.8 mm nozzle at 345 kPa. The printing process of the 3D-CTEG thermoelements, were performed at 30 mm s^{-1} on forward/backward order, creating 3 uniform layers. Each printed line of the SWCNT-based material was in contact with air for 0.9 to 4.5 ± 0.2 seconds before forming into an entire thermoelement. The SWCNT/epoxy-based thermoelements were cured in an oven at 100 °C for 2 hours, demonstrating a remarkable flexibility for an epoxy-based solid and cured material as shown in Fig. 1e and f. For high-grade 3D-printable materials with significant TE efficiency, it is essential to produce dispersions with qualitative characteristics such as the viscosity which significantly contributes to the self-standing printing during the additive manufacturing process.[36,37] Fig. 1 shows the production process and the 3D-printed SWCNT-based materials, as well as the additive manufacturing process towards the 3D-printed flexible thermoelements.

2.2. Fabrication of the 3D-CTEG module

A flexible carbon-based 3D-printed TEG device was manufactured *via* facile paste printing processes utilizing the produced materials, consisted of 2 p-/n-pairs. Fig. 2a, illustrates the additive manufacturing of TE module fabrication process. The 3D-CTEG p-/n-pair has the dimensions of 13 mm × 15 mm × 2.0 mm as indicated in Fig. 2b. Initially, p-type TE material was 3D-printed on a scaled PTFE/Teflon substrate in order to print-develop the device design architecture. Thereafter, n-type material printing was processed in the same way on the same substrate to alternate the carbon-based interconnection resulting in a continuous electric path composed of 2 p-/n-pairings. Copper foils were integrated directly while printing the p- and n-type carbon-based materials on top of the copper as the anode and cathode terminals of the device. All the thermoelements were cured at 100 °C for 120 minutes after printing. The 3D-printed highly-dense and conductive SWCNT network was also employed as electrodes/interconnections between the printed thermoelements, resulting in a carbon-based TEG that does not require metal deposition as it is also described in a previous study,[13] where the contact resistance between the metal electrode and the SWCNTs is larger in the case of highly electrically conductive SWCNTs than the resistance of the metal or the SWCNT itself, and as a result, the procedure adding metallic interconnections in large scale results in TEGs with lower power output.[38] The carbon-based 3D-printed TEG and its working principle are illustrated in Fig. 2c and d.

2.3. Characterization, thermoelectric properties and performance measurements

Surface morphological micrographs of the 3D-printed TE materials were taken using a Zeiss Gemini field emission scanning electron microscope (FE-SEM), operating at an accelerating voltage of 1.0 to 3.0 kV (Zeiss, Germany). In order to characterize the thermoelectric properties of the fabricated 3D-CTEG module, the performance and the thermal stability of the materials were carried out. The thermopower was generated by keeping one block "cold" at room temperature (*i.e.* $T_{ambient}$ ~ 25 °C) while heating the other at various temperatures.

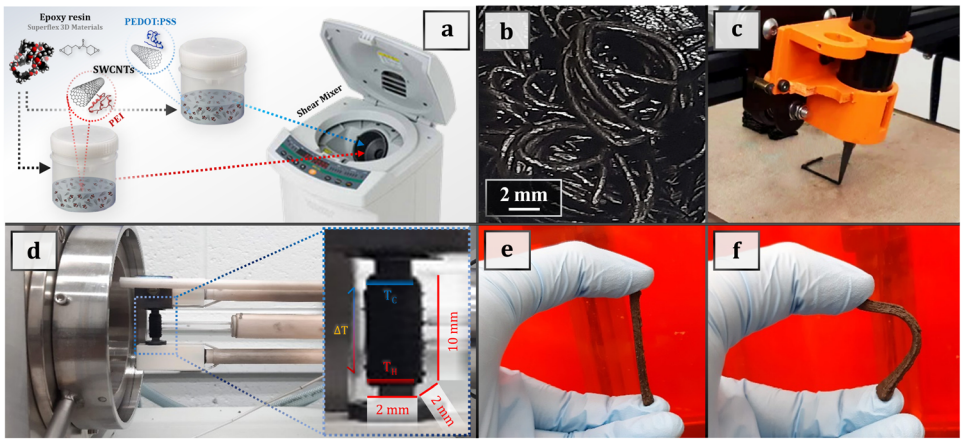

Fig. 1 Thermoelectric paste production process. (a) The dispersion process of the SWCNTs using a shear-mixer, (b) the produced p-type SWCNT/epoxy-based dispersion after extrusion printing, (c) the additive manufacturing process of thermoelements, (d) the thermoelectric characterization of the 3D-printed materials, and (e) and (f) the flexibility of the SWCNT/epoxy-based 3D-printed TE material after curing.

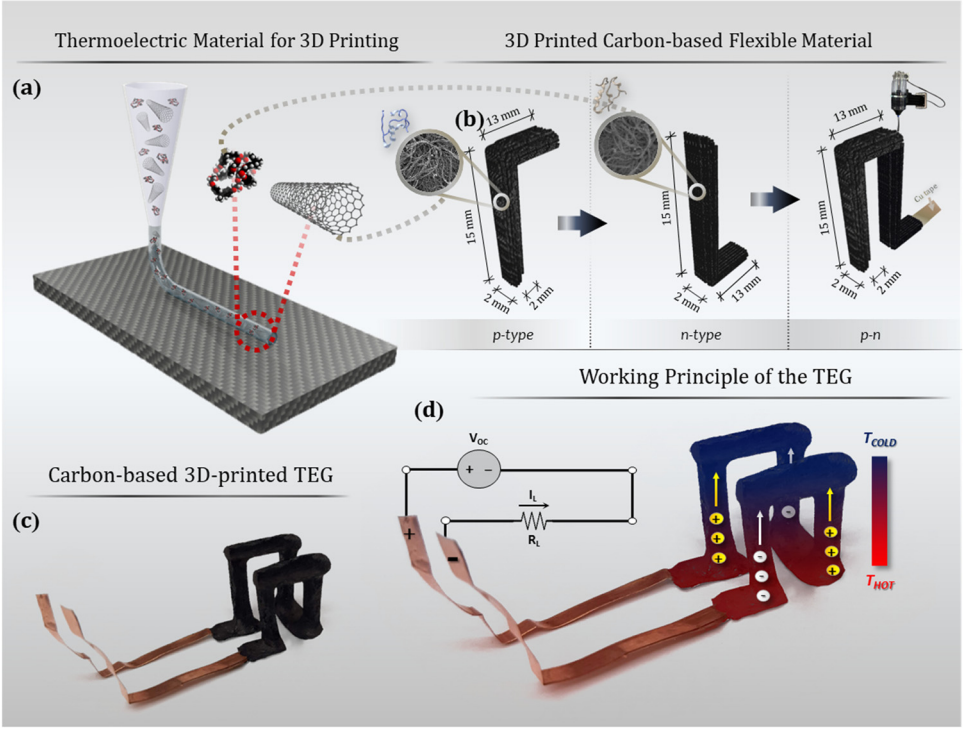

Fig. 2 Carbon-based 3D-printed flexible TEG manufacturing process. (a) Additive manufacturing process of the SWCNT/epoxy-based TE materials, (b) printing process and dimensions of the thermoelements of the CTEG device, (c) 3D-CTEG device architecture, (d) schematic illustration of the thermoelectrically generated carriers, by a given temperature difference (ΔT) as well as the 3D-CTEG's module working principle and the CTEG's equivalent circuit.

The measurements were performed in a laboratory environment at 1 atm pressure and relative humidity of 50 ± 5%. The temperatures of T_{Cold} and T_{Hot} blocks were continuously controlled by K-type thermocouples and a digital IR Thermometer OS-VIR50 (OMEGA Engineering Ltd, United Kingdom) for the accurate temperature difference (ΔT) monitoring. 3D-CTEG's current and voltage generated under various temperature differences, were measured using the 34401Agilent DMM (Agilent Technologies, USA). Viscosity measurements of the thermoelectric materials have been performed using the NDJ-9S digital viscometer. The efficiency and the performance of the flexible 3D-CTEG was computer-controlled by custom made LabVIEW programs in order to deliver the *V*–*I*, *P*–*I*, V–R_{LOAD} and P–R_{LOAD} curves.

The electrical conductivities, Seebeck coefficients, power factors and figure of merits (*ZT*s) of the 3D-printed SWCNT-based thermoelements were measured using the Linseis LSR-3 thermoelectric characterization instrument (Linseis, Germany). The reported values are average values from at least five measurements carried out on different samples. The thermal conductivities of the produced materials were determined utilizing the Linseis THB-100 instrument under various temperature differences (Linseis, Germany). The thermal behavior of the produced materials was examined by using the STA 409 CD thermogravimetric analyser from NETZSCH GmbH (Selb, Germany), where the specimens were placed in a ceramic crucible and heated up with a constant heating rate of 10 °C min^{-1} in an oxygen atmosphere under a constant gas flow of 60 ml min^{-1}.

3. Results and discussion

3.1. Thermoelectric properties and characterization of the developed materials

For the purpose of fabricating optimized p- and n-type 3D-printed thermoelectric structures, various SWCNT : additive mass ratios were investigated, initially utilizing flexible epoxy as a dispersion medium to create conductive 3D-printable inks, and then modified and investigated accordingly with various additive : mass-ratios to achieve preferable viscosity and thermoelectric characteristic to manufacture 3D flexible TEG architectures. In particular, Fig. 3a, illustrates the achieved viscosities of the developed thermoelectric TE materials at various epoxy : SWCNTs mass ratios at room temperature. The initial epoxy : SWCNTs developed material achieved the viscosity of 27 Pa s. Fig. 3b and c depicts the recorded Seebeck coefficients, power factors and electrical conductivities of the produced p- and n-type SWCNT TE materials at various mass ratios, measured as cured structures. While developing the SWCNT dispersions, the optimum ratio regarding the TE properties and the viscosity for the 3D-printing process were the 10 wt% of SWCNTs/20 wt% of PEDOT:PSS in the epoxy for the p-type, and 10 wt% of SWCNTs/15 wt% of PEI for the n-type

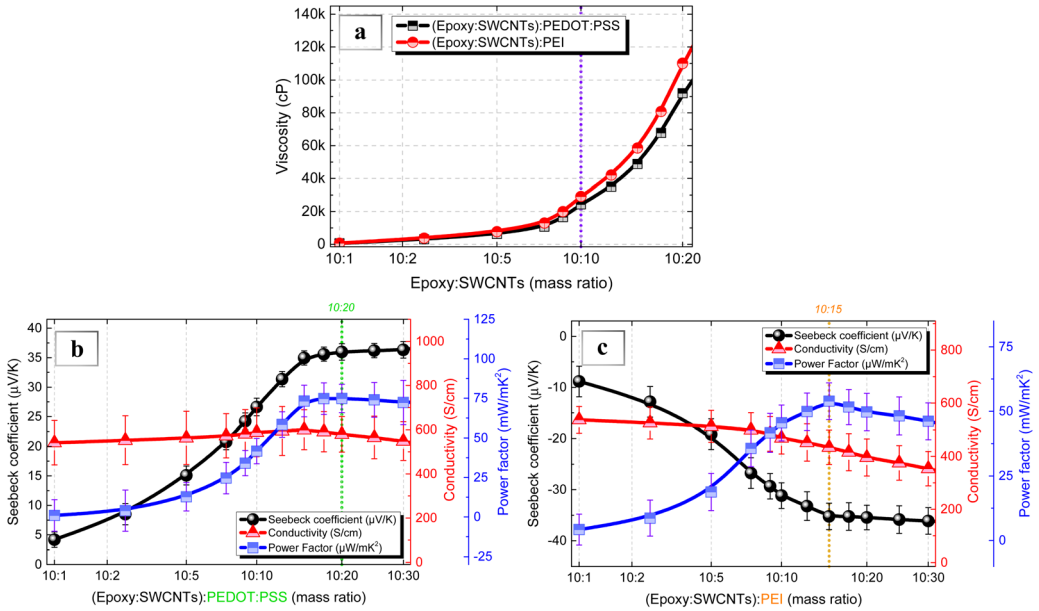

Fig. 3 Thermoelectric characterization of the 3D-printed TE materials. (a) Viscosities of the produced additive manufacturing SWCNT/epoxy-based TE materials at various mass ratios at room temperature, and (b) and (c) Seebeck coefficients, electrical conductivities, and power factors of the p- and n-type printed structures at various (Epoxy : SWCNTs) : Additive mass ratios.

material. As referred[15,33,39,40] and also observed in the this study, the use of PEDOT:PSS prevents nanotube-epoxy interactions and any unwanted n-doping modification due to the amine-groups containing in epoxy resins. For the n-type fabrication while using PEI, it has been investigated that when the mass ratio of PEI to SWCNTs exceeds 10 : 15, the Seebeck coefficient does not provide any significant enhancement while the electrical conductivity decreases significantly as more dielectric PEI molecules interact with the conductive nanotubes. Apart from being high-quality and homogeneous dispersions, the selected TE pastes, also exhibiting the quite satisfactory functional viscosities for 3D printing of 25 Pa s and 29 Pa s, for p- and n-type respectively, as shown in Fig. 3a. As a result, they may also be employed for large-scale printing processes.

In this study, environmentally friendly methods were acquired to produce TE pastes for facile 3D-printed applications, avoiding the use of heavy chemicals and strong acids for dopants as has been previously referred in other studies.[41,42] Fig. 3 depicts the electrical conductivities of 579 S cm^{-1} and 434 S cm^{-1} and the Seebeck coefficients of 36 μV K^{-1} and −35 μV K^{-1} were obtained of p- and n-type structures. As a result, the recorded PFs were as high as 75 μW mK^{-2} and 54 μW mK^{-2} at ΔT = 100 K for the developed p- and n-tsnype SWCNT-based flexible 3D-printed materials, respectively.

3.2. Thermogravimetric analysis of p- and n-type materials

Thermogravimetric analysis (TGA) was performed to evaluate their thermal performance and limitations of the 3D-printed p- and n-type SWCNT/epoxy-based TE materials. This thermal investigation demonstrates the capacity and stability of the produced 3D materials for low temperature applications up to 180 °C. Fig. 4a shows the thermal degradation of the materials in terms of their weight mass. Zone "I",

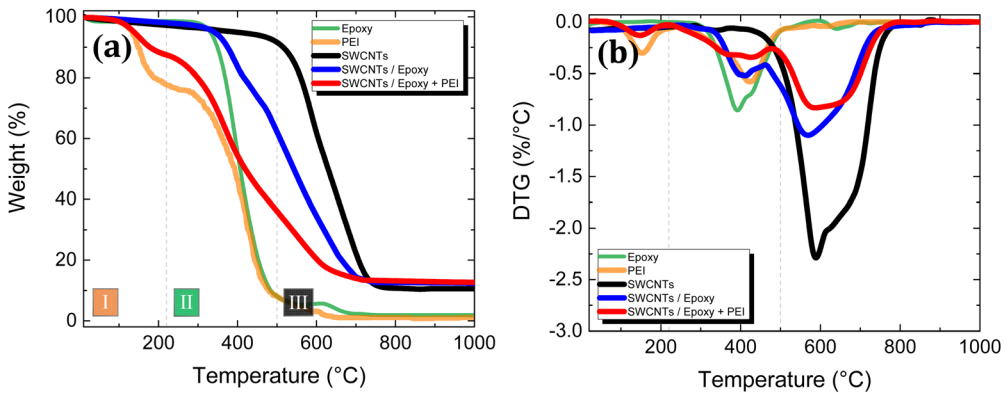

Fig. 4 (a) Thermogravimetric analysis (TGA) and (b) the derivative of TG (DTG) of p-type, n-type thermoelements, Epoxy, PEI and pristine SWCNTs.

represents the evaporation of water in each material (0–210 °C), whereas zone "II" indicates the initiation of polymer molecules burning (210–500 °C), and zone "III" illustrates the beginning of SWCNT degradation and also the combustion of the residual polymer molecules (500–1000 °C). This is also consistent with the initial SWCNTs as shown in Fig. 4a and b.

To summarize, the PEI-based n-type 3D-printed SWCNT/epoxy-based material, demonstrates a stable but highly depended to high-temperature limit at 180 °C, making it ideal for low-temperature applications, such as biothermal or wearable energy harvesting devices. The remaining ~15% of mass on SWCNT-based TGA samples is related to metal impurities produced during the nanotube fabrication process.[43]

3.3. Surface morphology and microscopy characterization of the 3D-printed materials

The solid-state morphology and the dispersion quality of the 3D-printed SWCNT/epoxy-based n- and p-type TE materials were investigated. Fig. 5 depicts the SEM images of the surface morphology of the n- and the p-type 3D-printed structures. As mentioned before, the SWCNT/epoxy mixtures were produced utilizing a shear-mixer at 2000 rpm, 3D-printed *via* DIW and cured at 100 °C for 2 hours. The three-dimensional printed structures demonstrate comparable dense-network structures that efficiently assist to carrier transports, implying to the functionalized thermoelectric dispersions of the produced n- and p-type materials. Fig. 5a and b illustrates the remarkable continuity of the SWCNT network of the p-type printed material. Fig. 5c and d shows the n-type printed structure, where an excellent doping of SWCNTs was established during the thermoelectric characterization as described in paragraph 3.4, confirming that adequate PEI molecules were bonded on the surfaces of the SWCNTs, leading in efficient doping due to the anion-induced electron transfer between the nitrogen anions (N^-) of PEI to the SWCNTs. In an earlier study, it is also mentioned the effective n-doping of utilizing PEI molecules on SWCNTs.[38,44,45]

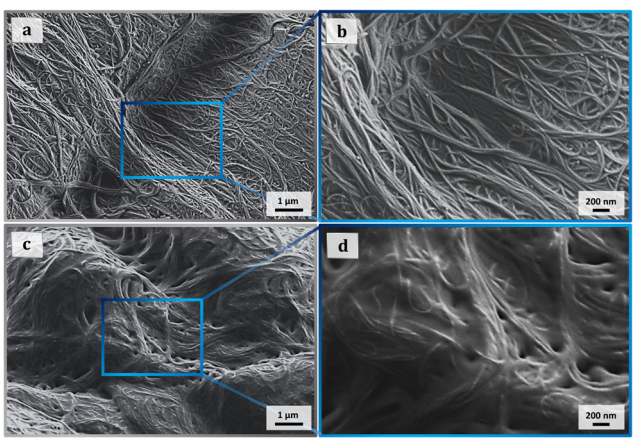

Fig. 5 (a) and (b) SEM micrographs of the p- and (c) and (d) n-type 3D-printed SWCNT/epoxy-based TE materials.

3.4. Thermoelectric characterization of the carbon nanotube-based 3D printed materials

The thermoelectric characteristics of the SWCNT/epoxy-based 3D-printed materials were thoroughly investigated. More specifically, the σ: electrical conductivity, S: Seebeck coefficient, PF: power factor, κ: thermal conductivity, zT: figure of merit, and η: thermoelectric efficiency of the 3D-printed materials were measured or evaluated as a function of temperature. The dimensionless figure of merit (zT) of a TE material that is used to describe the TE efficiency is equal to[11]:

$$zT = \frac{\sigma S^2 T}{\kappa} \quad (1)$$

where σ, S, κ, are as described above, and T is the absolute temperature. For a TE material, the ideal efficiency of thermal to electrical energy conversion is stated as:[46]

$$\eta = \left(\frac{T_H - T_C}{T_H}\right)\frac{\sqrt{1+Z\bar{T}}-1}{\sqrt{1+Z\bar{T}}+(T_C/T_H)} \quad (2)$$

The Carnot efficiency is described by the first factor in (2). The second factor specifies how much Carnot efficiency may be produced from a TEG under a certain ΔT, which is a function of $Z\bar{T}$. T_H denotes the temperature at the hot surface, whereas T_C denotes the continuous temperature of a cool surface. The temperature differential ($T_H - T_C$) of a TE material is defined by the temperatures on its hot side (T_H) and cold side (T_C), and $\bar{T}$ is the average of these values.

Fig. 6a and b depicts the TE performance of the p-/and n-type SWCNT/epoxy-based materials as a function of T. The remarkable values of 620 S cm^{-1} and 471 S cm^{-1}, as well as the significantly high S values of 41 µV K^{-1} and −40 µV K^{-1} at T = 180 °C are notable. As a consequence, the 3D-printed p- and n-type SWCNT/epoxy-based TE materials have the substantial PFs of 102 µW mK^{-2} and 75 µW mK^{-2}, respectively. The obtained κ values for the 3D-printed TE structures are 0.174 W mK^{-1} and 0.132 W mK^{-1} for the p- and n-type materials, respectively, and decline as the temperature rises, which is consistent with earlier findings, reaching the values of 0.09 W mK^{-1} and 0.07 W mK^{-1} respectively at T = 180 °C.[13,47,48] Ultimately, the significant zT of 0.52 and 0.47 at T = 180 °C give remarkable conversion efficiencies of η = 3.4% and η = 2.9% for the p- and n-type TE materials respectively. These values herald a quite promising future of additive manufacturing in thermoelectrics, as they arise from abundant, low-cost, flexible carbon-based and facile to manufacture materials.

3.5. Performance and demonstration of the 3D-CTEG device

The fabricated 3D-CTEG device exhibited a significant thermoelectric performance, due to the excellent characteristics of the n- and p-type 3D-printed materials, manufactured employing the SWCNT/epoxy-based semiconducting materials *via* DIW method. When the 3D-CTEG module is exposed to a ΔT between the device's top and bottom sides (through-thickness), a significant power output is generated. The experimentally measured TE performance of the 3D-CTEG device in multiple

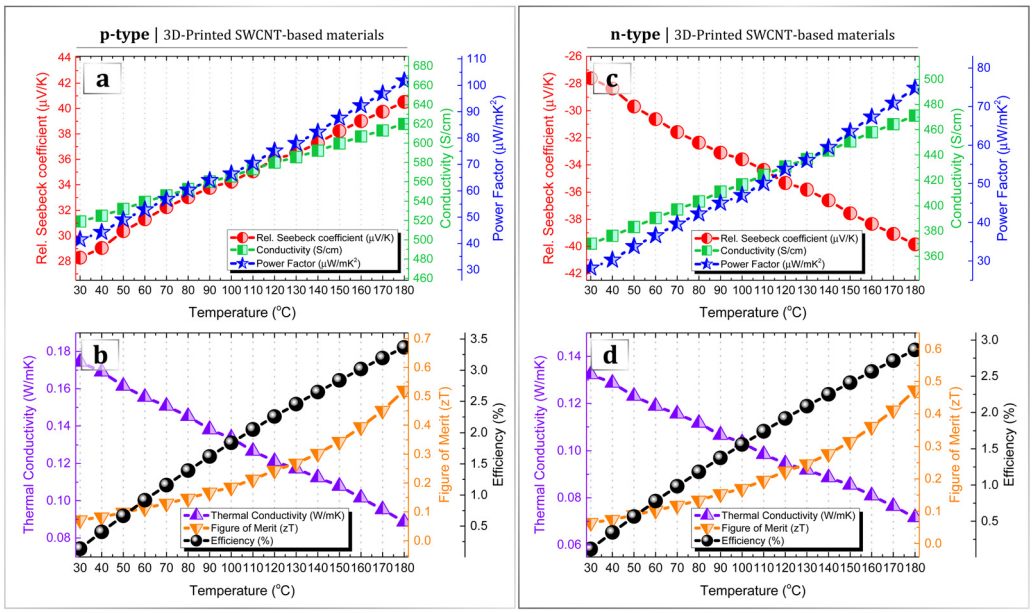

Fig. 6 Thermoelectric characterization and properties of the 3D-printed SWCNT-based materials. (a) and (c) The measured Seebeck coefficients, electrical conductivities, power factors, and (b) and (d) thermal conductivities, zT and thermoelectric efficiencies of (a) and (b) p- and (c) and (d) n-type epoxy-dispersed nanotube-based TE materials respectively at various temperatures.

ΔTs is illustrated in Fig. 7. The measurements were conducted under standard laboratory conditions (T: 25 °C, RH: ~50%, 1 atm). The printed architecture of the flexible 3D-CTEG having the dimensions of 13 mm × 13 mm × 15 mm, demonstrated a total thermopower of 136 μV K^{-1} at ΔT = 100 K. It should be noted that the fabricated 3D-CTEG displayed an excellent TE performance for each thermoelement without the need of metallic interconnections. This result was achieved due to the superior conductivity of the SWCNT-based 3D-printed materials, as well as the short distance between the linked thermoelements. As has been referred in a previous study, the contact resistance of a metallic interconnection and a printed nanotube-based structure is larger than the internal resistance of either a metal or a SWCNT-based structure alone, resulting in a reduced power output.[13,38] This is not the case with our 3D-CTEG, which is made entirely of SWCNTs with high electrical conductivity. At ΔT = 100 K, a V_{OC} = 13.6 mV (open-circuit voltage) and an I_{SC} = 740 μA (short-circuit current) were obtained during the 3D-CTEG performance measurements with an internal resistance R_{TEG} = 11.3 Ohm. This resulted in a significant power output of 4.1 μW, as can be seen in Fig. 7 and 8.

The power density of the 3D-CTEG module could be calculated using the equation.[49]

$$P_{\text{density}} = \frac{P_{\max}}{N \cdot A} = \frac{(N \cdot S \cdot \Delta T)^2 / 4 \cdot N \cdot \dfrac{l}{\sigma \cdot w \cdot d}}{N \cdot w \cdot d} = \frac{S^2 \cdot \sigma}{4l} \cdot \Delta T^2 \quad (3)$$

where N represents the number of the thermoelements, A is the area of the thermoelement, w is the width, d is the thickness and l is the length of the thermoelements. The power density of the 3D-CTEG was calculated at 256 mW m^{-2} and the specific

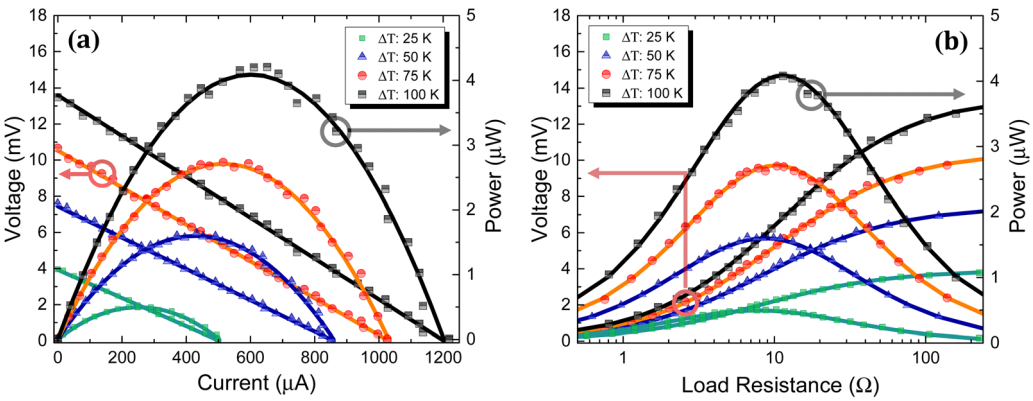

Fig. 7 The experimentally measured thermoelectric performance of the 3D-CTEG in various ΔTs. (a) The obtained curves of voltage–current (V–I), power–current (P–I) and (b) voltage–load resistance (V–R_{LOAD}), power–load resistance (P–R_{LOAD}).

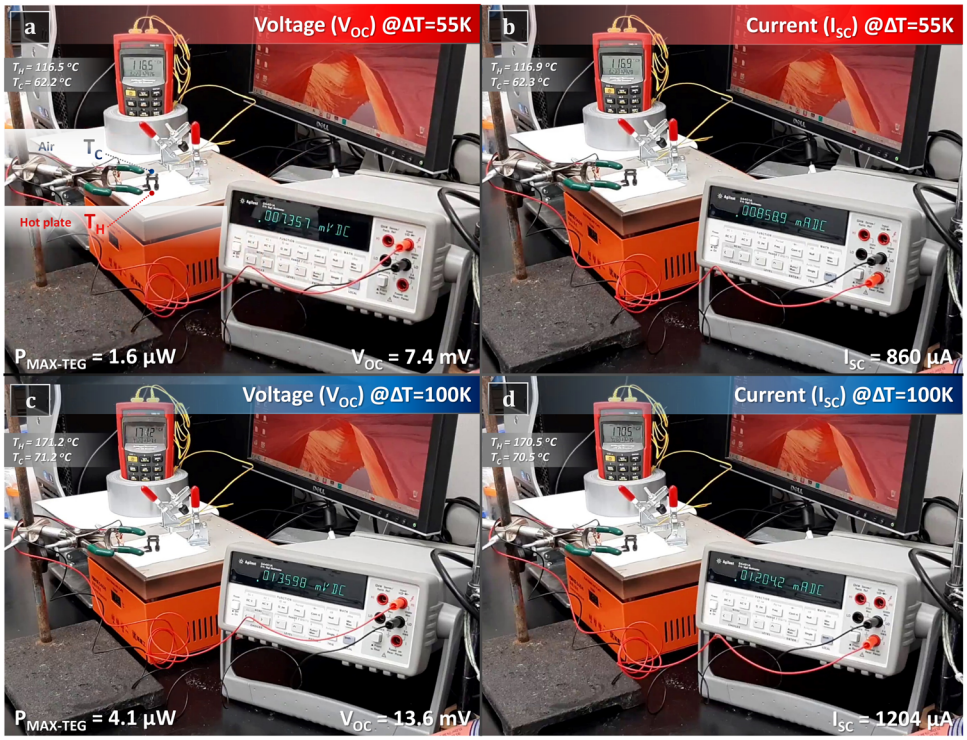

Fig. 8 3D-CTEG-device performance. The generated open-circuit voltage (V_{OC}) and short-circuit current (I_{SC}) at (a, b) ΔT = 55 K and (c, d) at ΔT = 100 K.

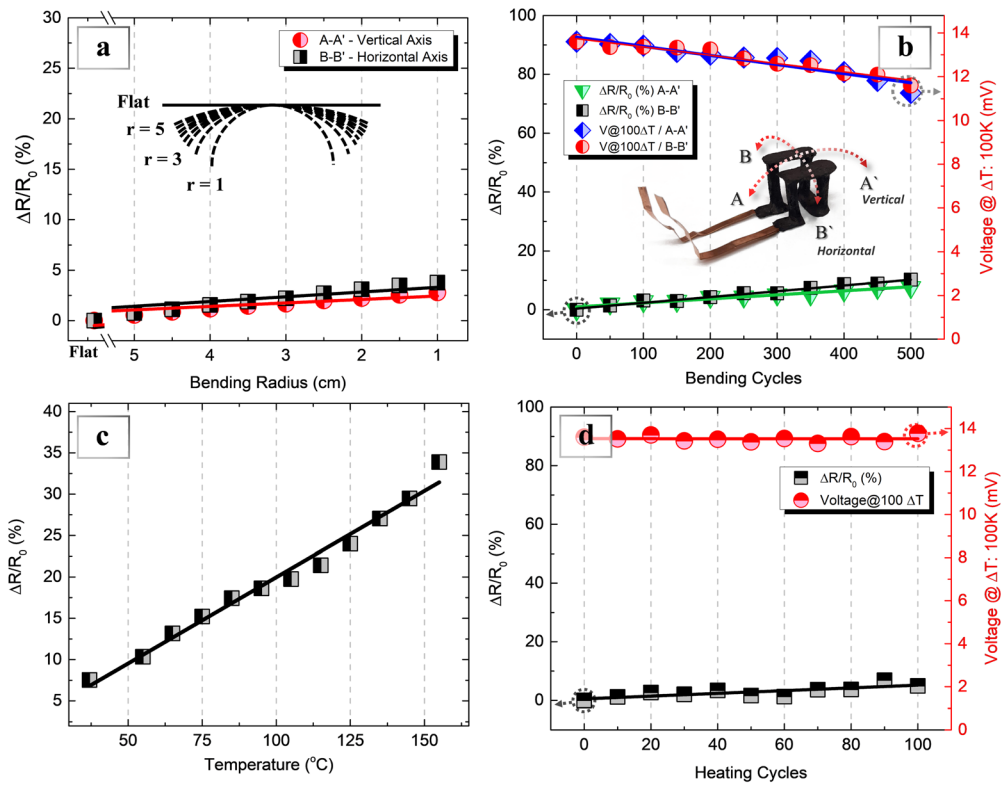

Fig. 9 Flexibility measurements of the developed 3D-CTEG device. (a) Resistance variation ratios ($\Delta R/R_0$) of the CTEG while bending with different radii. (b) $\Delta R/R_0$ and voltage output in various bending cycles @ΔT = 100 °C. (c) $\Delta R/R_0$ as a temperature function. (d) The repeatability of the $\Delta R/R_0$ as well as the voltage output of the CTEG over 100 heating cycles at ΔT =100 °C. For (b)–(d) the bending radius was 2 cm.

power at 205 μW g^{-1}, both of which are amid the highest values reported for flexible 3D-printed TEGs.[7,35,44,50,51]

3.6. Flexibility performance of the 3D-CTEG structure

Quantitative assessment of the bending radius of the manufactured structure was performed by bending the 3D-CTEG device. The flexibility of the TEG device is quite important for the endurance and integrity of the module's performance and functionality. Additionally, it could be useful to understand the possibilities and limitations for the device to be applicable to heat sources with irregular surfaces to take advantage of the ubiquitous heat dissipation. Conventional π-type TE modules consist of p-/n-type TE materials electrically interconnected in-series *via* metal contacts. Furthermore, numerous gold or silver nanometers are often placed as top electrodes on each thermoelement to minimize contact resistance. In contrast to a standard TEG configuration, our 3D-CTEG lacks rigid metallic contacts between p-type and n-type thermocouples, resulting in exceptional flexibility, as illustrated in Fig. 9. Fig. 9a depicts the variation of resistance $\Delta R/R_0$ of the manufactured 3D-CTEG as a function of bending radius ranging from 5 cm to 1 cm in the vertical (A–A') and horizontal axis (B–B'). The resistance variation ratio is expressed as $\Delta R/R_0$, where R_0 is the 3D-CTEG device's initial resistance and ΔR is the resistance change between the real-time resistance measured under specific function and R_0 ($\Delta R = R - R_0$). When the 3D-CTEG was flexed along A–A' and B–B' axes up to a radius of 1 cm, the structure's $\Delta R/R_0$ was 2.9% and 3.8%, respectively; contrary, the overall internal resistance change was trivial. Fig. 9b depicts the $\Delta R/R_0$ *versus* the obtained voltage after numerous bending iterations with a radius of 2 cm. Following 500 bending cycles, the unit's $\Delta R/R_0$ values were 7.6% along the A–A' axis and 10.3% at the B–B' axis. During this time, the device's output voltage at ΔT = 100 °C (T_H = 170 °C), was nearly constant. The $\Delta R/R_0$ *versus* the device's temperature rise is shown in Fig. 9c, where an almost linear trend is observed, with an average rise of 2.4% every 10 °C. The 3D-CTEG's durability is demonstrated in Fig. 9d, where the device's generated voltage and internal resistance both remained remarkably constant after a 100 heating cycle evaluation. In summary, the manufactured 3D-CTEG device is shown to have exceptional durability, stability, and flexibility, making it a reliable thermoelectric generator.

4. Conclusions

This study has the aim to utilize additive manufacturing *via* DIW method to develop a carbon-based flexible 3D-printed thermoelectric generator and demonstrate its TE performance. The SWCNT/epoxy-based TE material employed for the printed TEG architecture is based on SWCNT/epoxy dispersions and produced *via* facile shear-mixing methods and low-cost materials. The manufactured 3D-CTEG consisted of two serially interconnected carbon-based p-/n-pairs. Due to their excellent electrical conductivity, the SWCNT/epoxy-based printed TE structures were also adopted for connectors between the p-/n- thermoelements. The dominant p- and n-type 3D-printed TE materials, demonstrated the substantial PFs of 102 μW mK^{-2} and 75 μW mK^{-2} respectively. The additively manufactured 3D-CTEG exhibited a V_{OC} = 13.6 mV and an I_{SC} = 1204 μA at ΔT = 100 K with an R_{TEG} = 11.3 Ω. As an outcome, the noteworthy power output of 4.1 μW was achieved by only four thermoelements. The fabrication of a flexible 3D-CTEG with thermal energy harvesting capabilities is a key step toward sustainable and sophisticated zero-energy consumption components and constructions. This particular thermoelectric device development approach could easily be adjusted in wearables (shoes, jacket insulation mesh), transportation (car hoods, heated parts of aircrafts or ships), and even existing power generation devices (basis of photovoltaic devices in direct contact with the panels, or even wind turbine thermal spots).

It is also a potentially efficient method for a broad range of applications, including distant places where powering low-energy consumption devices is required to give entirely energy independent solutions. The substantially obtained TE efficiency attained by the carbon-based 3D-TEG expands immense for large-scale 3D-ptintable and additive manufacturing processes of low-cost and efficient flexible thermoelectric generators, which might have a significant influence on the renewable energy sector.

Author contributions

C. K. M. was involved to the production processes of the thermoelectric materials, the device architecture, the principal idea and the implementation of the design, the manufacturing, and the characterization of the 3D-CTEG. W. J. W. contributed to the 3D-printing additive manufacturing processes of the carbon-based TE materials. C. K. M., R. G. and L. T. involved to the thermoelectric and electrical characterization of the produced materials. C. K. M., A. S. P. and E. C. involved to the core idea development. C. K. M. and L. T. involved to the TGA measurements and analysis of the 3D-printed materials. C. K. M. involved to the SEM measurements, imaging and analysis. A. S. P. and E. C. also contributed to advising, reviewing, editing and supervise the entire study.

Conflicts of interest

There are no conflicts to declare.

Acknowledgements

C. K. M. gratefully acknowledges the Fulbright Foundation and the Institute of International Education (iie) for financial support of this research at the College of Engineering of the University of Miami.

References

1 R. Sivaraj, P. K. S. M. Rahman, P. Rajiv, H. A. Salam and R. Venckatesh, Biogenic copper oxide nanoparticles synthesis using Tabernaemontana divaricate leaf extract and its antibacterial activity against urinary tract pathogen, *Spectrochim. Acta, Part A*, 2014, **133**, 178–181.

2 M. G. Kanatzidis, in Chapter 3 The role of solid-state chemistry in the discovery of new thermoelectric materials, ed. T. M. Tritt, *Semiconductors and Semimetals*, Elsevier, 2001, pp. 51–100.

3 A. J. Minnich, M. S. Dresselhaus, Z. F. Ren and G. Chen, Bulk nanostructured thermoelectric materials: current research and future prospects, *Energy Environ. Sci.*, 2009, **2**(5), 466–479.

4 M. Aljaghtham and E. Celik, Design of cascade thermoelectric generation systems with improved thermal reliability, *Energy*, 2022, **243**, 123032.

5 G. Tan, L.-D. Zhao and M. G. Kanatzidis, Rationally Designing High-Performance Bulk Thermoelectric Materials, *Chem. Rev.*, 2016, **116**(19), 12123–12149.

6 X.-L. Shi, J. Zou and Z.-G. Chen, Advanced Thermoelectric Design: From Materials and Structures to Devices, *Chem. Rev.*, 2020, **120**(15), 7399–7515.

7 C. Oztan, S. Ballikaya, U. Ozgun, R. Karkkainen and E. Celik, Additive manufacturing of thermoelectric materials *via* fused filament fabrication, *Appl. Mater. Today*, 2019, **15**, 77–82.

8 M. Aljaghtham and E. Celik, Energy conversion and thermal reliability of thermoelectric materials in unileg annular configuration, *Mater. Lett.*, 2021, **300**, 130192.

9 G. Zhou and D. Wang, Few-quintuple Bi2Te3 nanofilms as potential thermoelectric materials, *Sci. Rep.*, 2015, **5**(1), 8099.

10 C. Y. Oztan, B. Hamawandi, Y. Zhou, S. Ballikaya, M. S. Toprak, R. M. Leblanc, V. Coverstone and E. Celik, Thermoelectric performance of Cu2Se doped with rapidly synthesized gel-like carbon dots, *J. Alloys Compd.*, 2021, **864**, 157916.

11 G. J. Snyder and A. H. Snyder, Figure of merit ZT of a thermoelectric device defined from materials properties, *Energy Environ. Sci.*, 2017, **10**(11), 2280–2283.

12 Q. Jiang, J. Yang, P. Hing and H. Ye, Recent advances, design guidelines, and prospects of flexible organic/inorganic thermoelectric composites, *Mater. Adv.*, 2020, **1**(5), 1038–1054.

13 C. K. Mytafides, L. Tzounis, G. Karalis, P. Formanek and A. S. Paipetis, High-Power All-Carbon Fully Printed and Wearable SWCNT-Based Organic Thermoelectric Generator, *ACS Appl. Mater. Interfaces*, 2021, **13**(9), 11151–11165.

14 G. Karalis, L. Tzounis, K. Tsirka, C. K. Mytafides, M. Liebscher and A. S. Paipetis, Carbon fiber/epoxy composite laminates as through-thickness thermoelectric generators, *Compos. Sci. Technol.*, 2022, 109291.

15 C. K. Mytafides, L. Tzounis, K. Tsirka, G. Karalis, M. Liebscher, E. Lambrou, L. N. Gergidis and A. S. Paipetis, A hierarchically modified fibre-reinforced polymer composite laminate with graphene nanotube coatings operating as an efficient thermoelectric generator, *Mater. Adv.*, 2024, **5**, 3721–3734.

16 T. Juntunen, H. Jussila, M. Ruoho, S. Liu, G. Hu, T. Albrow-Owen, L. W. T. Ng, R. C. T. Howe, T. Hasan, Z. Sun and I. Tittonen, Inkjet Printed Large-Area Flexible Few-Layer Graphene Thermoelectrics, *Adv. Funct. Mater.*, 2018, **28**(22), 1800480.

17 F. Kim, B. Kwon, Y. Eom, J. E. Lee, S. Park, S. Jo, S. H. Park, B.-S. Kim, H. J. Im, M. H. Lee, T. S. Min, K. T. Kim, H. G. Chae, W. P. King and J. S. Son, 3D printing of shape-conformable thermoelectric materials using all-inorganic Bi2Te3-based inks, *Nat. Energy*, 2018, **3**(4), 301–309.

18 R. R. Søndergaard, M. Hösel, N. Espinosa, M. Jørgensen and F. C. Krebs, Practical evaluation of organic polymer thermoelectrics by large-area R2R processing on flexible substrates, *Energy Sci. Eng.*, 2013, **1**(2), 81–88.

19 Y. Jia, Q. Jiang, H. Sun, P. Liu, D. Hu, Y. Pei, W. Liu, X. Crispin, S. Fabiano, Y. Ma and Y. Cao, Wearable Thermoelectric Materials and Devices for Self-Powered Electronic Systems, *Adv. Mater.*, 2021, **33**(42), 2102990.

20 J. Zang, J. Chen, Z. Chen, Y. Li, J. Zhang, T. Song and B. Sun, Printed flexible thermoelectric materials and devices, *J. Mater. Chem. A*, 2021, **9**(35), 19439–19464.

21 C. Navone, M. Soulier, M. Plissonnier and A. L. Seiler, Development of (Bi,Sb)2(Te,Se)3-Based Thermoelectric Modules by a Screen-Printing Process, *J. Electron. Mater.*, 2010, **39**(9), 1755–1759.

22 A. Chen, D. Madan, P. K. Wright and J. W. Evans, Dispenser-printed planar thick-film thermoelectric energy generators, *J. Micromech. Microeng.*, 2011, **21**(10), 104006.

23 M. He, Y. Zhao, B. Wang, Q. Xi, J. Zhou and Z. Liang, 3D Printing Fabrication of Amorphous Thermoelectric Materials with Ultralow Thermal Conductivity, *Small*, 2015, **11**(44), 5889–5894.

24 D. Grossin, A. Montón, P. Navarrete-Segado, E. Özmen, G. Urruth, F. Maury, D. Maury, C. Frances, M. Tourbin, P. Lenormand and G. Bertrand, A review of additive manufacturing of ceramics by powder bed selective laser processing (sintering/melting): Calcium phosphate, silicon carbide, zirconia, alumina, and their composites, *Open Ceram.*, 2021, **5**, 100073.

25 M. Manoj Prabhakar, A. K. Saravanan, A. Haiter Lenin and I. Jerin, leno, K. Mayandi, P. Sethu Ramalingam, A short review on 3D printing methods, process parameters and materials, *Mater. Today Proc.*, 2021, **45**, 6108–6114.

26 Y. Yan, H. Ke, J. Yang, C. Uher and X. Tang, Fabrication and Thermoelectric Properties of n-Type CoSb2.85Te0.15 Using Selective Laser Melting, *ACS Appl. Mater. Interfaces*, 2018, **10**(16), 13669–13674.

27 Y. Mao, Y. Yan, K. Wu, H. Xie, Z. Xiu, J. Yang, Q. Zhang, C. Uher and X. Tang, Non-equilibrium synthesis and characterization of n-type Bi2Te2.7Se0.3 thermoelectric material prepared by rapid laser melting and solidification, *RSC Adv.*, 2017, **7**(35), 21439–21445.

28 M. Smith, Z. Guan and W. J. Cantwell, Finite element modelling of the compressive response of lattice structures

manufactured using the selective laser melting technique, *Int. J. Mech. Sci.*, 2013, **67**, 28–41.
29 S. Iijima, Helical Microtubules of Graphitic Carbon, *Nature*, 1991, **354**, 56.
30 Y. Shi, C. Yan, Y. Zhou, J. Wu, Y. Wang, S. Yu and Y. Chen, in Chapter 1 - Overview of additive manufacturing technology and materials, ed Y. Shi, C. Yan, Y. Zhou, J. Wu, Y. Wang, S. Yu, Y. Chen, *Materials for Additive Manufacturing*, Academic Press, 2021, pp. 1–8.
31 G. Karalis, L. Tzounis, E. Dimos, C. K. Mytafides, M. Liebscher, A. Karydis-Messinis, N. E. Zafeiropoulos and A. S. Paipetis, Printed Single-Wall Carbon Nanotube-Based Joule Heating Devices Integrated as Functional Laminae in Advanced Composites, *ACS Appl. Mater. Interfaces*, 2021, **13**(33), 39880–39893.
32 C. K. Mytafides, L. Tzounis, G. Karalis, P. Formanek and A. S. Paipetis, Fully printed and flexible carbon nanotube-based thermoelectric generator capable for high-temperature applications, *J. Power Sources*, 2021, **507**, 230323.
33 G. Karalis, L. Tzounis, K. Tsirka, C. K. Mytafides, A. Voudouris Itskaras, M. Liebscher, E. Lambrou, L. N. Gergidis, N.-M. Barkoula and A. S. Paipetis, Advanced Glass Fiber Polymer Composite Laminate Operating as a Thermoelectric Generator: A Structural Device for Micropower Generation and Potential Large-Scale Thermal Energy Harvesting, *ACS Appl. Mater. Interfaces*, 2021, **13**(20), 24138–24153.
34 Y. Nonoguchi, K. Ohashi, R. Kanazawa, K. Ashiba, K. Hata, T. Nakagawa, C. Adachi, T. Tanase and T. Kawai, Systematic Conversion of Single Walled Carbon Nanotubes into n-type Thermoelectric Materials by Molecular Dopants, *Sci. Rep.*, 2013, **3**, 3344.
35 J. L. Blackburn, A. J. Ferguson, C. Cho and J. C. Grunlan, Carbon-Nanotube-Based Thermoelectric Materials and Devices, *Adv. Mater.*, 2018, **30**(11), 1704386.
36 K. Chiou, S. Byun, J. Kim and J. Huang, Additive-free carbon nanotube dispersions, pastes, gels, and doughs in cresols, *Proc. Natl. Acad. Sci. U. S. A.*, 2018, **115**(22), 5703–5708.
37 K. Suganuma, *Introduction to Printed Electronics*, Springer, Osaka, Japan, 2014.
38 J. Choi, Y. Jung, S. J. Yang, J. Y. Oh, J. Oh, K. Jo, J. G. Son, S. E. Moon, C. R. Park and H. Kim, Flexible and Robust Thermoelectric Generators Based on All-Carbon Nanotube Yarn without Metal Electrodes, *ACS Nano*, 2017, **11**(8), 7608–7614.
39 G. Karalis, K. Tsirka, L. Tzounis, C. Mytafides, L. Koutsotolis and A. S. Paipetis, Epoxy/Glass Fiber Nanostructured p- and n-Type Thermoelectric Enabled Model Composite Interphases, *Appl. Sci.*, 2020, **10**(15), 5352.
40 G. Karalis, C. K. Mytafides, L. Tzounis, A. S. Paipetis and N.-M. Barkoula, An Approach toward the Realization of a Through-Thickness Glass Fiber/Epoxy Thermoelectric Generator, *Materials*, 2021, **14**(9), 2173.
41 J. L. Blackburn, T. M. Barnes, M. C. Beard, Y.-H. Kim, R. C. Tenent, T. J. McDonald, B. To, T. J. Coutts and M. J. Heben, Transparent Conductive Single-Walled Carbon Nanotube Networks with Precisely Tunable Ratios of Semiconducting and Metallic Nanotubes, *ACS Nano*, 2008, **2**(6), 1266–1274.
42 R. C. Tenent, T. M. Barnes, J. D. Bergeson, A. J. Ferguson, B. To, L. M. Gedvilas, M. J. Heben and J. L. Blackburn, Ultrasmooth, Large-Area, High-Uniformity, Conductive Transparent Single-Walled-Carbon-Nanotube Films for Photovoltaics Produced by Ultrasonic Spraying, *Adv. Mater.*, 2009, **21**(31), 3210–3216.
43 S. G. King, L. McCafferty, V. Stolojan and S. R. P. Silva, Highly aligned arrays of super resilient carbon nanotubes by steam purification, *Carbon*, 2015, **84**, 130–137.
44 W. Zhou, Q. Fan, Q. Zhang, L. Cai, K. Li, X. Gu, F. Yang, N. Zhang, Y. Wang, H. Liu, W. Zhou and S. Xie, High-performance and compact-designed flexible thermoelectric modules enabled by a reticulate carbon nanotube architecture, *Nat. Commun.*, 2017, **8**(1), 14886.
45 J.-H. Mo, J.-Y. Kim, Y. H. Kang, S. Y. Cho and K.-S. Jang, Carbon Nanotube/Cellulose Acetate Thermoelectric Papers, *ACS Sustainable Chem. Eng.*, 2018, **6**(12), 15970–15975.
46 G. J. Snyder and E. S. Toberer, Complex thermoelectric materials, *Nat. Mater.*, 2008, **7**(2), 105–114.
47 R. S. Prasher, X. J. Hu, Y. Chalopin, N. Mingo, K. Lofgreen, S. Volz, F. Cleri and P. Keblinski, Turning Carbon Nanotubes from Exceptional Heat Conductors into Insulators, *Phys. Rev. Lett.*, 2009, **102**(10), 105901.
48 Y. Lan, Y. Wang and Z. Ren, Physics and applications of aligned carbon nanotubes, *Adv. Phys.*, 2011, **60**, 553–678.
49 Y. Lu, Y. Ding, Y. Qiu, K. Cai, Q. Yao, H. Song, L. Tong, J. He and L. Chen, Good Performance and Flexible PEDOT:PSS/Cu2Se Nanowire Thermoelectric Composite Films, *ACS Appl. Mater. Interfaces*, 2019, **11**(13), 12819–12829.
50 M.-H. Lee, Y. H. Kang, J. Kim, Y. K. Lee and S. Y. Cho, Freely Shapable and 3D Porous Carbon Nanotube Foam Using Rapid Solvent Evaporation Method for Flexible Thermoelectric Power Generators, Advanced Energy, *Materials*, 2019, **9**(29), 1900914.
51 D. Zhang, W. Y. S. Lim, S. S. F. Duran, X. J. Loh and A. Suwardi, Additive Manufacturing of Thermoelectrics: Emerging Trends and Outlook, *ACS Energy Lett.*, 2022, **7**(2), 720–735.